JAMES | Journal of Advances in Modeling Earth Systems

RESEARCH ARTICLE
10.1029/2023MS004136

Evaluating Numerical Methods to Investigate Spectral Solar Radiative Transfer in Plant Canopies

Zachary Moon[1,2] **and Jose D. Fuentes**[1]

[1]Department of Meteorology and Atmospheric Science, The Pennsylvania State University, University Park, PA, USA, [2]Earth Resources Technology, Inc., Laurel, MD, USA

Key Points:

- Disposition of spectral sunlight in plant canopies is important to understand photolysis of molecules amenable to absorbing light
- Spectral resolution is required to estimate reliable estimates of air chemistry-specific quantities related to photolysis of molecules
- A waveband resolution of at least 10 nm is sufficient to obtain accurate estimates for most photochemical reactions

Supporting Information:

Supporting Information may be found in the online version of this article.

Correspondence to:

J. D. Fuentes,
jdfuentes@psu.edu

Citation:

Moon, Z., & Fuentes, J. D. (2024). Evaluating numerical methods to investigate spectral solar radiative transfer in plant canopies. *Journal of Advances in Modeling Earth Systems*, *16*, e2023MS004136. https://doi.org/10.1029/2023MS004136

Received 20 NOV 2023
Accepted 15 JUN 2024

Author Contributions:

Conceptualization: Zachary Moon, Jose D. Fuentes
Data curation: Zachary Moon, Jose D. Fuentes
Formal analysis: Zachary Moon, Jose D. Fuentes
Funding acquisition: Zachary Moon, Jose D. Fuentes
Investigation: Zachary Moon, Jose D. Fuentes
Methodology: Zachary Moon, Jose D. Fuentes
Project administration: Zachary Moon, Jose D. Fuentes

Abstract The disposition of spectral solar irradiance in plant canopies is crucially important to understand processes such as photolysis of molecules amenable to absorbing actinic light. Thus, one objective of this study is to evaluate the most commonly applied radiative transfer approaches to estimate spectral irradiance as a function of plant canopy depth. Eight radiative transfer approaches are ascertained. Another objective is to determine the impacts of the spectral resolution assumed in radiative transfer calculations and model choice on key processes such as canopy absorption and reflection of irradiance. By comparing results from broadband-only and spectrally-resolved canopy radiative transfer, we aim to quantitatively determine the uncertainties associated with failing to resolve the sunlight spectra. We determine the optimal spectral resolution required to estimate canopy radiative transfer results such as air-chemistry-specific quantities related to photolysis of a select group of molecules. In addition, we evaluate techniques for binning leaf and soil optical properties. Results showed that high spectral resolution is ideally desired to compute photolysis of molecules such as ozone, nitrogen dioxide, nitrate radical, nitrous acid, and formaldehyde. For in-canopy photolysis of molecules, a waveband resolution of at least 10 nm is sufficient to obtain accurate estimates for most photochemical reactions. Positive reaction-dependent uncertainties in canopy-mean relative photolysis values for individual molecules can be as high as 30% compared to estimates derived with broad-band solar irradiance.

Plain Language Summary In regions dominated by tall and dense forest canopies, climate models need to resolve the vertical variation of sunlight to estimate assimilation of gases by foliage. Knowledge of sunlight disposition in forest canopies is also needed to determine light-driven reactions of gases. Most climate models employ broadband sunlight to determine radiative transfer in plant canopies. Given that in-plant canopy processes such as reactions of gases require knowledge of sunlight specified at high wavelength resolution, eight different radiative transfer models are considered to discern the most reliable approach to compute the disposition of solar radiation as a function of both canopy depth and wavelength. Results indicate it is necessary to estimate the in-canopy disposition of sunlight as a function of wavelength to reliably compute dissociation of molecules susceptible to sunlight absorption. As part of the light spectra included in radiative transfer numerical models, a waveband resolution of at least 10 nm is necessary to reduce uncertainties of less than 30% of sunlight-mediated dissociation of molecules such as ozone and nitrogen dioxide. The new approach developed in this study can be included in numerical modeling systems designed to investigate photochemical processes in vegetated landscapes.

1. Introduction

Radiative transfer (RT) in plant canopies is an important process to represent in land surface models. Canopy RT determines how much global solar energy is reflected (albedo) and how much is absorbed by canopy (foliage and stem) elements and the ground (soil) surface. Despite its importance, relatively few studies have compared the performance and physics of RT approaches commonly included in one-dimensional (1-D) numerical models. The RAMI4PILPS project (RAdiation transfer Model Intercomparison (RAMI) for the Project for Intercomparison of Land-Surface Parameterizations; Widlowski et al., 2011) evaluated the performance of several models, comparing results to a reference (Raytran, a 3-D Monte Carlo ray-tracing model; Govaerts & Verstraete, 1998) identified in the main RAMI experiments (Widlowski et al., 2007, 2015). However, the assessed approaches (their Table 2) were, for the most part, more complex than the 1-D approaches commonly included in regional/global land models such as the Community Land Model Version 5, CLM5 (Lawrence et al., 2019). Previous studies (Y. P. Wang, 2003) compared three approaches (i.e., Goudriaan's method (Goudriaan, 1977), a Beer–Lambert-based model (Campbell & Norman, 2012), and the two-stream approximation (Dickinson, 1983; Sellers, 1985))

Software: Zachary Moon, Jose D. Fuentes
Validation: Zachary Moon, Jose D. Fuentes
Visualization: Zachary Moon, Jose D. Fuentes
Writing – original draft: Zachary Moon, Jose D. Fuentes
Writing – review & editing: Zachary Moon, Jose D. Fuentes

commonly used in determining the RT in plant canopies included in land surface models. However, those studies did not examine differences in spectrally resolved irradiance profiles in plant canopies. Instead, they considered the broadband irradiances such as photosynthetically active radiation (PAR) or near-infrared (NIR). As evident in foliage optical properties (Serbin & Townsend, 2020) and modeled profiles of spectral irradiance (Moon et al., 2020), the relative degree of in-canopy sunlight extinction depends on wavelength. As a result, not all sunlight wavelengths are uniformly modified by foliage elements in the plant canopy. Modeling broad bands of irradiance does not account for these non-uniform changes in foliage radiative characteristics across the sunlight wavelengths, which arise due to finer-scale wavelength dependencies in the leaf and soil optical properties (Vane & Goetz, 1988; Jacquemoud & Baret, 1990; R. Braghiere et al., 2023).

This study investigates the transfer of *spectral* irradiance in plant canopies utilizing a newly developed software system named CRT1D (Canopy Radiative Transfer, 1-D). Resolving the ultraviolet-visible (UV-Vis) part of the sunlight spectrum is essential for computing photolysis of molecules (throughout the article, photolysis denotes the dissociation of molecules by photons of sunlight) from first principles (Moon et al., 2020). In addition, the numerical modeling of plant canopy photosynthetic rates depend on both temporal structure of the sunlight dosage (Gu et al., 1999; Kivalov & Fitzjarrald, 2018, 2019) and spectral irradiance (Gu et al., 2019) as carbon dioxide assimilation is not linearly related to wavelengths and saturates at high sunlight levels. The RT spectral resolution impacts fundamental processes such as sunlight reflectivity, transmissivity, and absorptivity as a function of canopy depth. It is fundamentally critical to resolve the spectral irradiance to more reliably estimate amounts of absorbed and reflected irradiance, which are crucial components of the surface energy balance (van der Tol et al., 2009). Furthermore, based on spectral radiative transfer in plant canopies and inverse methods, it is possible to identify plant functional traits such as pigment, water, and nitrogen content in foliage (Ollinger & Smith, 2005; Serbin & Townsend, 2020).

In applications such as remote sensing of vegetated surfaces, it has been recognized that the disposition of the sunlight spectrum within plant canopies is crucial to investigate ecophysiological processes. Canopy RT models employed by the remote sensing community dealing with vegetated landscapes include spectral resolution sufficient to resolve the major features of the leaf and soil optical property spectra. Since the advent of "hyperspectral" remote sensing (waveband $\lesssim$10-nm resolution), relevant wavelength-dependent radiance information has become more readily available to study a myriad of ecological processes (R. Braghiere et al., 2023). For instance, remote sensing of solar-induced chlorophyll fluorescence (SIF), a proxy for foliage photosynthetic activity, requires spectrally resolved sunlight data (Gu et al., 2019; Mohammed et al., 2019). One representative and widely used example model that includes spectral irradiance is PROSAIL (Jacquemoud et al., 2009), which combines the PROSPECT leaf optical properties model (PROperty SPECTra; Feret et al., 2008, 1-nm resolution) and the SAIL (Scattering by Arbitrary Inclined Leaves; Verhoef, 1984) canopy reflectance model. However, standalone 1-D canopy micro-environment and canopy-atmosphere models, and canopy RT modules included in the land components of regional/global 3-D numerical weather prediction and climate models have included only two (PAR and NIR) or three (adding UV) broad wavelength bands of sunlight. One exception is the SCOPE model (Soil Canopy Observation of Photosynthesis and Energy fluxes; van der Tol et al., 2009) that uses a variable-resolution wavelength grid, including 1-nm resolution in the 400–2,400 nm spectral region. Although the SCOPE model is intended for use in remote sensing, it considers chlorophyll fluorescence in addition to standard canopy RT. Because SIF activity depends on photosynthesis, which in turn depends on canopy and leaf temperatures (and other variables), the canopy physical micro-environment must be modeled as well. Nevertheless, the impact of spectral resolution on modeled quantities in SCOPE has not been explicitly evaluated. The Climate Modeling Alliance land model, CliMA-Land (R. K. Braghiere et al., 2021; Y. Wang et al., 2021), with many components based on mSCOPE (multilayer SCOPE, a version which allows vertical variation of leaf biochemical and biophysical properties; P. Yang et al., 2017), also resolves the sunlight spectrum within the canopy with a variable wavelength grid (5-, 10-, or 25-nm resolution within the 400–2,400 nm spectral region). As with SCOPE, the sensitivity to spectral resolution has not been investigated. Moreover, only limited field observations (e.g., Baldocchi et al., 1984; Chen, 1996; Staebler et al., 1997) have been made to characterize the vertical and horizontal variability of radiative transfer in plant canopies whose sunlight interactions (e.g., transmitted and absorbed sunlight levels) strongly depend upon canopy structure, that is, plant height and density and vertical leaf area distribution (Parker et al., 2019).

In 1-D numerical models, the disposition of actinic light in plant canopies is ordinarily determined based on RT approaches involving broadband irradiance. The earlier plant canopy photochemical models ("canopy-chemistry"

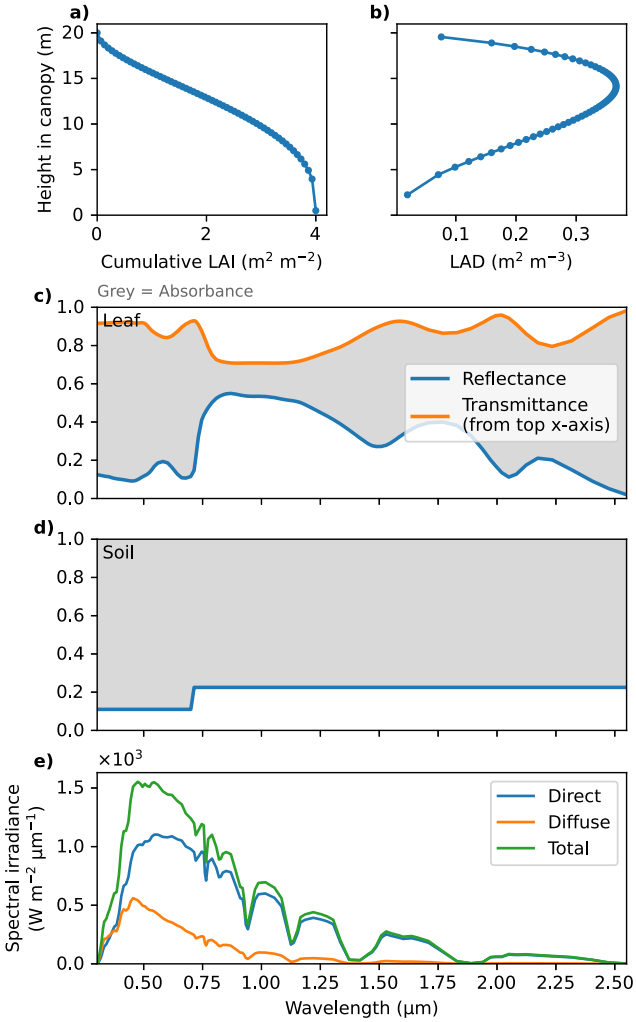

Figure 1. Cumulative leaf area index and leaf area density (LAD) profiles (a, b), leaf and ground surface optical properties (c, d), and top-of-canopy spectral irradiance (e) for the CRT1D default case. The wavelengths span from 0.3 to 2.6 μm. The gray fill represents the absorbance fraction in (c) and (d).

models; e.g., J. D. Fuentes et al., 2007, 2022; Gao et al., 1993; Hu et al., 2015; Makar et al., 1999; Stroud et al., 2005; Wolfe & Thornton, 2011) relied on the Beer–Lambert radiative transfer approach to compute in-canopy photolysis of molecules. The canopy-chemistry model by Saylor (2013) originally included a Beer–Lambert-type method (Irmak & Mutiibwa, 2008) but was later updated to include sunlight scattering and absorption by canopy layers (Bodin & Franklin, 2012). Other canopy-chemistry models (Ashworth et al., 2015; Forkel et al., 2006) employed the radiative transfer approach developed by Norman (1979) that is described in Section 2.1.2.

Regional/global land models such as the CLM5 (Lawrence et al., 2019) and 1-D canopy (non-chemistry) models employ similar radiative transfer methods. For example, the 1-D multilayer version of CLM (CLM-ml v0, G. B. Bonan et al., 2018) includes three approaches: the two-stream approximation (Dickinson, 1983; Sellers, 1985), that of Goudriaan (1977), and the one from Norman (1979). The canopy RT scheme for the canopy model Cupid is described in Norman (1979). Canopy RT for the CANOAK model (Baldocchi et al., 1984) is based on Norman (1979) as well. Utilizing the two-stream approximation in a 1-D model (Hogan et al., 2018), examined the 3-D interactions of solar irradiance with vegetation canopies, generating comparable results to the ones derived from the RAMI4PILPS intercomparison project. The cited previous numerical models apply shortwave canopy RT and partition the global solar irradiance into the UV, PAR, and NIR bands.

The majority of land and 1-D canopy(-chemistry) models do not include spectrally resolved radiative transfer in plant canopies. Instead, they employ two or three broad wavelength bands to estimate assimilation of carbon dioxide or calculate photolysis of molecules. However, two bands alone clearly cannot well-resolve the shortwave leaf optical property spectra (Figure 1c; Serbin & Townsend, 2020). Although in Moon et al. (2020) high spectral resolution was used to compute photolysis of molecules within a plant canopy, that study did not evaluate the impacts of waveband spectral resolution on the *sensitivity* of the calculated photolysis of molecules. Therefore, three research objectives frame the scope of the current study. First, we identify and seek to assess the performance of the most suitable RT approaches included in land models to estimate the spectral irradiance as a function of plant canopy depth to investigate photochemical processes of chemical species amenable to photolysis (Moon et al., 2020). Second, the optimal spectral resolution of sunlight required to reliably estimate the canopy RT is ascertained by contrasting results such as total canopy reflected irradiance and photolysis of selected molecules. Finally, techniques for binning leaf and soil optical properties are developed to include in the RT methods evaluated in the present study. Features of the CRT1D software, such as tools for manipulating sunlight spectra, creating initial/boundary conditions, plotting/analysis routines for comparing results, and diagnostic routines for the computation of various absorption variables and integrals over certain wavelength bands, are employed to achieve the research objectives.

2. Research Methods

2.1. Radiative Transfer Methods

The CRT1D tool was originally developed to study the disposition of the light spectrum and photochemical reactions in plant canopies (Moon et al., 2020). The CRT1D includes the RT models of Norman (1979) (as described in G. Bonan (2019)), Bodin and Franklin (2012), Goudriaan (1977) (as described by Bodin and Franklin (2012)), and Zhao and Qualls (2005) (as implemented in the Python version of the APES model (Launiainen et al., 2015, https://github.com/LukeEcomod/pyAPES_skeleton)). Table 1 provides names and abbreviations of the canopy RT methods used in this study. The first four methods listed in Table 1 are described

Table 1
Canopy RT Schemes Currently Included in CRT1D

Method abbreviation	Description	References
B–L	Beer–Lambert	Campbell and Norman (2012), Monteith and Unsworth (2013)
2s	Dickinson–Sellers two-stream	Dickinson (1983), Sellers (1985)
4s	Four-stream	Tian et al. (2007)
ZQ	Zhao and Qualls multi-scattering	Zhao and Qualls (2005)
BF	Bodin and Franklin	Bodin and Franklin (2012)
G77	Goudriaan (1977)	Goudriaan (1977), Bodin and Franklin (2012)
ZQ-pA	Zhao and Qualls from pyAPES	Zhao and Qualls (2005), Launiainen et al. (2015)
N79	Norman (1979)	Norman (1979)

in Moon et al. (2020), see their Equations 8–10. In the following, we describe the salient features of the remaining approaches.

The included RT methods can be grouped in different ways in order to highlight the differences in their application. One grouping approach is based on the numerical solution type. Most models are based on analytical solutions to the radiative transfer equation, formulated by making assumptions and approximations about the primitive canopy RT relationships. The ZQ (+ZQ-pA) and N79 methods (Table 1), however, also involve numerical approximations of in-canopy layer scattering and absorption, introducing a dependence on the number of vertical layers used in the model. The other methods utilize continuous profiles derived from analytical solutions to their RT equation and so are not sensitive to the vertical resolution. Another grouping approach relies on the complexity of handling light scattering. The more complex models such as 2s, 4s, ZQ, ZQ-pA, and N79 (Table 1) estimate in-canopy multiple scattering and provide the upward diffuse light profile as part of the RT solution. The B–L, BF, and G77 models either do not provide an upward diffuse light profile or the treatment of in-canopy multiple scattering is much simpler, leading to significant differences in the upward diffuse light profile.

2.1.1. The G77 and BF Models

The G77 approach is similar to that of the B–L method described in Campbell and Norman (2012). Its formulation does not include a profile of upwelling irradiance. Its implementation in CRT1D is based on the description provided in Bodin and Franklin (2012). Similar to 2s and B–L, the G77 and BF methods make simplifications about light scattering that allow analytical solutions to the RT problem. In the G77 method, the continuous downwelling diffuse light profile ($I^{\downarrow}(\mathrm{L})$) is estimated based on the incoming diffuse irradiance measured above the plant canopy $\left(I^{\downarrow}_{\mathrm{sky},d}\right)$, applying the Beer–Lambert-style expression:

$$I^{\downarrow}(L) = I^{\downarrow}_{\mathrm{sky},\,d}\, e^{-k_d L} = I^{\downarrow}_{\mathrm{sky},\,d}\, \tau_d(L) \tag{1}$$

where L is the cumulative leaf area index (LAI) from the top of the canopy and k_d is an extinction coefficient for diffuse irradiance. The coefficient k_d within the canopy is modeled using the diffuse bulk transmissivity

$$\tau_d = 2\int_0^{\frac{\pi}{2}} \tau_b(\psi, L)\sin(\psi)\cos(\psi)\, d\psi \tag{2}$$

using $\tau_b(\psi, L) = e^{-k_b(\psi)L}$, which is the black-leaf transmissivity for the direct solar beam. The ψ is the solar zenith angle (SZA). For method self-consistency, in Equation 1, CRT1D does not include the multiplicative $(1 - \rho_c)$ factor used by Bodin and Franklin (2012), where ρ_c is the canopy reflectance. The factor would make the downward diffuse incorrect at the top of the canopy ($L = 0$). The G77 model also computes a profile of diffuse light due to scattering, but does not specify the direction; the G77 model as formulated in Goudriaan (1977) and presented in G. Bonan (2019) does not give solutions for the upward and downward light streams, only for layerwise absorbed light.

The BF model (Bodin & Franklin, 2012) builds upon G77 method, adding terms to account for the upwelling light stream, providing separate expressions for upward and downward streams associated with scattered direct beam irradiance. In the BF approach, the downwelling diffuse profile is given by the sum of direct beam irradiance scattered downwards ($I_{sc\downarrow}(L)$) and diffuse transmission $\left(I_d^{\downarrow}(L)\right)$:

$$\begin{aligned} I^{\downarrow}(L) &= I_{sc\downarrow}(L) + I_d^{\downarrow}(L) \\ &= I_{\text{sky},\,b}^{\downarrow}\,\tau_{\ell}\frac{\tau_b(L)-\tau_d(L)}{k_d-k_b} + I_{\text{sky},\,d}^{\downarrow}\,\tau_d(L) \end{aligned} \tag{3}$$

where $\tau_b(L)$ is the direct beam transmittance from the top of the canopy to depth L, τ_{ℓ} is the (single) leaf transmittance, and k_b is the direct solar beam extinction coefficient ($\tau_b = e^{-k_b L}$, neglecting clumping). The upwelling diffuse is given by the sum of direct beam irradiance scattered upwards and ground surface reflectance:

$$\begin{aligned} I^{\uparrow}(L) &= I_{sc\uparrow}(L) + I_{sr\uparrow} \\ &= I_{\text{sky},\,b}^{\downarrow}\,\rho_{\ell}\frac{\tau_b - e^{k_d L-(k_d+k_b)L_{\text{tot}}}}{k_d+k_b} + \rho_s\left[I_{\text{sky},\,b}^{\downarrow}\,\tau_b(L_{\text{tot}}) + I^{\downarrow}(L_{\text{tot}})\right]e^{-k_d(L_{\text{tot}}-L)} \end{aligned} \tag{4}$$

where ρ_{ℓ} is the (single) leaf reflectance and ρ_s is the ground surface albedo (Bodin & Franklin, 2012). The $I_{\text{sky},d}$ and $I_{\text{sky},\,b}$ variables are the diffuse and direct radiative fluxes at the top of the canopy, respectively.

2.1.2. The N79 Method

The N79 method (Norman, 1979), like ZQ, uses numerical approximation techniques to solve a coupled system of layerwise upward and downward diffuse radiative fluxes. In the N79 method, the downward and upward diffuse radiation streams incident on leafy layer i are defined by

$$I_i^{\downarrow} = I_{i+1}^{\downarrow}\left[\tau_{d,\,i+1} + (1-\tau_{d,\,i+1})\tau_{\ell,i+1}\right] + I_i^{\uparrow}\left[(1-\tau_{d,\,i+1})\rho_{\ell,\,i+1}\right] + I_{\text{sky},\,b}^{\downarrow}\left[\mathrm{T}_{b,\,i+1}(1-\tau_{b,\,i+1})\right]\tau_{\ell,\,i+1} \tag{5}$$

$$I_{i+1}^{\uparrow} = I_i^{\uparrow}\left[\tau_{d,\,i+1} + (1-\tau_{d,\,i+1})\tau_{\ell,\,i+1}\right] + I_{i+1}^{\downarrow}\left[(1-\tau_{d,\,i+1})\rho_{\ell,\,i+1}\right] + I_{\text{sky},\,b}^{\downarrow}\left[\mathrm{T}_{b,\,i+1}(1-\tau_{b,\,i+1})\right]\rho_{\ell,\,i+1} \tag{6}$$

where τ_d is the layerwise diffuse light transmittance, τ_{ℓ} is the leaf light transmittance, ρ_{ℓ} is the leaf reflectance, and T_b is the transmissivity of the direct beam from top-of-canopy to the given layer. The $I_i^{\downarrow}$ variable is the downward radiative flux onto layer i, $I_{i+1}^{\uparrow}$ is the upward radiative flux leaving layer $i+1$, and $I_{\text{sky},b}^{\downarrow}$ is the top-of-canopy direct radiative flux. Here, i increases with height, not canopy depth, such that layer $i = N$ is the canopy-atmosphere interface layer. In Equation 5, the three terms represent (a) diffuse light transmission, including unscattered light penetration through the leaves between interface layers $i+1$ and i and (forward) scattering; (b) diffuse radiation reflected (scattered backward) while traveling upward from i to $i+1$; and (c) direct solar beam transmission, including unscattered light penetration and forward scattering. Norman (1979) described an iterative technique to solve Equation 5/6, but CRT1D uses the method outlined in G. Bonan (2019), in which a tridiagonal system of equations is constructed that can be easily solved in two sweeps using the well-known tridiagonal matrix algorithm (Press, 2007). In the tridiagonal system, there are $2(N+1)$ equations, where N is the number of layers. The $+1$ is needed to express the lower boundary conditions. G. Bonan (2019) provides a description of the elements of the tridiagonal matrix (see Equations 14.40–46). The RT solution is sensitive to the number of layers. For each canopy layer, Norman (1979) recommends a maximum LAI thickness of 0.5 $m^2\ m^{-2}$. In the CRT1D default case, following (Moon et al., 2020) a total LAI of 4 $m^2\ m^{-2}$ is split evenly into 60 layers, giving layer LAI values of $\ll$0.5 $m^2\ m^{-2}$.

2.2. The Default Radiative Transfer Parameterization

Unless otherwise noted, results shown in this study use the setup illustrated by Figure 1. The leaf area profile is a beta distribution with 60 layers, assuming a total LAI of 4.0 $m^2\ m^{-2}$ distributed from the top of the canopy to 0.5 m above the forest floor (Figure 1b). The studied forest had 0.5 m of bare trunk (Neumann et al., 1989). The simplified soil spectrum is based on J. D. Fuentes et al. (2007). As in Moon et al. (2020), we use ideal green leaf

optical properties (Figure 1c) based on published results (see Figure 6.5 in Monteith and Unsworth (2013)). The incoming spectral irradiances (Figure 1e) are the defaults in the SPCTRAL2 (Bird & Riordan, 1986) Excel version (available at https://www.nrel.gov/grid/solar-resource/spectral.html) and correspond to a clear day in the mid-latitudes near local solar noon. Additionally, the default SZA (ψ) is 20° and the default mean leaf inclination angle is 57°. The latter is approximately the value for the spherical leaf angle distribution, which is defined by the distribution function $f(\theta_l) = \sin\theta_l$ (e.g., Ross, 1981; X. Yang et al., 2023) and has a mean θ_l of 1 rad, or ≈57.2958°. It is important to note that this setup is idealized and is not intended to represent a particular vegetated research site. Rather, the goal is to provide results typical for a midlatitude deciduous forest during the middle of the growing season. During this time of full leaf-out and maximum leaf greenness, canopy radiative transfer can be relevant to processes such as carbon assimilation by leaves and photochemical reactions. Additional details beyond the default radiative transfer case studies are provided in Supporting Information S1.

2.3. Binning Spectral Irradiance

One goal of this study is to be able to easily examine the effect of spectral resolution on canopy RT results. In order to do this, it is necessary to interpolate the spectrally distributed quantities to the wavelength grid of interest. However, especially for spectra that are not very smooth, using traditional linear or spline interpolation methods can lead to inaccuracies. Furthermore, when binning irradiance, it is desirable to preserve the original total irradiance (integration over all wavelengths) as well as the spectrum shape. Thus, special methods are required.

One numerical method for binning spectra is the `inter2` routine from the Tropospheric Ultraviolet and Visible radiation model (TUV; Madronich & Flocke, 1997). This method will hereafter be referred to as the "TUV smear," inspired by the name given to it within the codebase of the F0AM model (Wolfe et al., 2016). The TUV smear works by computing the trapezoidal integral of the input spectrum over the desired bins. Each bin can have fractional contributions from multiple trapezoids based on how much they overlap that bin. For each bin i, defined by bounds $[x_{l,i}, x_{u,i})$, we have that

$$\frac{\int_{x_{l,i}}^{x_{u,i}} y_0(x)\,dx}{x_{u,i} - x_{l,i}} = y_i \tag{7}$$

where $\int$ represents the trapezoidal integral, $y_0(x)$ is the original spectrum, and y_i is the binned value within bin i. Thus, for the binned spectrum, the integral is conserved. That is,

$$\sum_i^N y_i\,\delta x_i = \mathrm{trapz}\big(y_0(x)\big) \tag{8}$$

where δx are the bin widths ($\delta x_i = x_{u,i} - x_{l,i}$). This equality will only hold of course if the leftmost bin edge to the rightmost spans the range of x values in the original spectrum.

For irradiance, it is important to bin the spectral irradiance values (W m^{-2} μm^{-1}) rather than in-bin integrated irradiances (W m^{-2}) so that the total spectrally integrated irradiance is properly conserved. In-bin irradiance values, if needed, are calculated after binning the spectral irradiance by multiplying by the wavelength bin widths ($\delta\lambda_i$).

2.4. Binning Optical Properties

For leaf and ground surface optical properties, the TUV smear alone is insufficient because average optical properties in a given spectral region also depend on the spectra (diffuse and direct) of the illuminating light in that spectral region. Reflectance and transmittance are defined relative to the incoming radiant flux as the fraction of the incoming light that is reflected or transmitted at a certain wavelength. Therefore, within a given bin, the ideal representative optical property value will be weighted more toward the values of its spectrum where the light intensity is greater; wavelengths where there is relatively less light contribute less to the bin value. Simply using the TUV smear does not account for this effect.

At a certain wavelength, λ, leaf reflectance $r_l(\lambda) = I_r(\lambda)/I_i(\lambda)$, where I_i is the incoming light intensity (here, incoming solar irradiance) and I_r the reflected. Over a waveband, as in Equation 7, we have

$$r_{l,i} = \frac{\int_{x_{l,i}}^{x_{u,i}} I_r(x)\,dx}{\int_{x_{l,i}}^{x_{u,i}} I_i(x)\,dx} \tag{9}$$

From a reflectance spectrum alone, $I_i(\lambda)$ and $I_r(\lambda)$ cannot be recovered. We can, however, make assumptions about $I_i(\lambda)$. With I_i known, $I_r = r_l I_i$. This allows us to compute $r_{l,i}$ as a weighted integral (in practice, a weighted average).

$$r_{l,i} = \frac{\int_{x_{l,i}}^{x_{u,i}} r_l(x) I_i(x)\,dx}{\int_{x_{l,i}}^{x_{u,i}} I_i(x)\,dx} \tag{10}$$

In this work, four different methods are used to bin the optical properties:

1. *TUV smear*. This method does not account for the incoming light spectrum and is included as a control or reference. This is akin to an average of $r_l(\lambda)$ over each bin.
2. *Light-weighted correction factor (Planck)*. This method starts from the binned optical properties spectrum of method 1. Using a light spectrum to provide weights, a single weighted average value of the optical properties is computed over all bins, adding weights ($I_i(x)$ in Equation 10) given by Planck black-body spectral irradiance (Since the weights are derived from an irradiance spectrum, this is effectively an energy-weighted average). By default, the Planck black-body irradiance spectrum used in this study has an absolute temperature (T) of $T = 6000$ K. This weighted average for the current binning is then compared to the value computed using the original leaf reflectance spectrum, representing the "known" broadband value. The ratio (original weighted average to weighted average with current bins) is used as a multiplicative correction factor (single correction factor for the whole set of bins).
3. *Light-weighted smear (Planck)*. Within each bin, a Planck irradiance spectrum shape is used to provide weights ($I_i(x)$ in Equation 10) during the smearing process. For the case of binning a spectrum to a single bin, this is equivalent to method 2.
4. *Light-weighted smear (realistic spectrum)*. A more realistic light spectrum (Figure 1e direct + diffuse irradiance) is used to provide weights.

It is important to recognize that the incoming top-of-canopy solar spectrum shape is not always the same. Even when considering only clear skies, wavelength-dependent attenuation will cause changes in the shape of the spectrum as path lengths of solar beams vary with SZA (time of day, time of year). Clouds and precipitation can cause even larger modifications to the light spectrum shape. Ideally, regional and global land models should incorporate this effect, computing new PAR and NIR (near-IR) optical properties based on the shape of the incoming solar spectrum, as done in Method 4. However, solar irradiance modules commonly used in regional and global atmospheric models, such as RRTMG (the Rapid Radiative Transfer Model for GCMs; Iacono et al., 2008), do not usually resolve the spectrum with a high level of detail (RRTMG has 9 bands in the wavelength region of Figure 1).

2.5. Light Absorption Calculations

Although some canopy RT methods (such as G77 and BF) include equations for computing absorbed irradiance in their formulations, in CRT1D, layerwise absorption is calculated as a post-processing step using the canopy RT outputs (the irradiance profiles). This means that, in CRT1D, differences in layerwise absorbed irradiance are only due to differences in the canopy RT solution and not caused by differences in absorption formulations.

It is important to recognize that the canopy RT solutions (upward and downward light streams) are valid at *interface* levels (e.g., the canopy-atmosphere interface is the topmost interface level). Absorption, however, occurs between these interface levels. It is useful to define representative *mass* levels between the interface levels at which the absorption variables are considered to be valid. In CRT1D, we use the LAI midpoints, consistent with G. Bonan (2019):

$$L_m(z_{m,i}) = [L(z_i) + L(z_{i+1})]/2 \quad \text{for} \quad i = 1,\ldots,N-1 \tag{11}$$

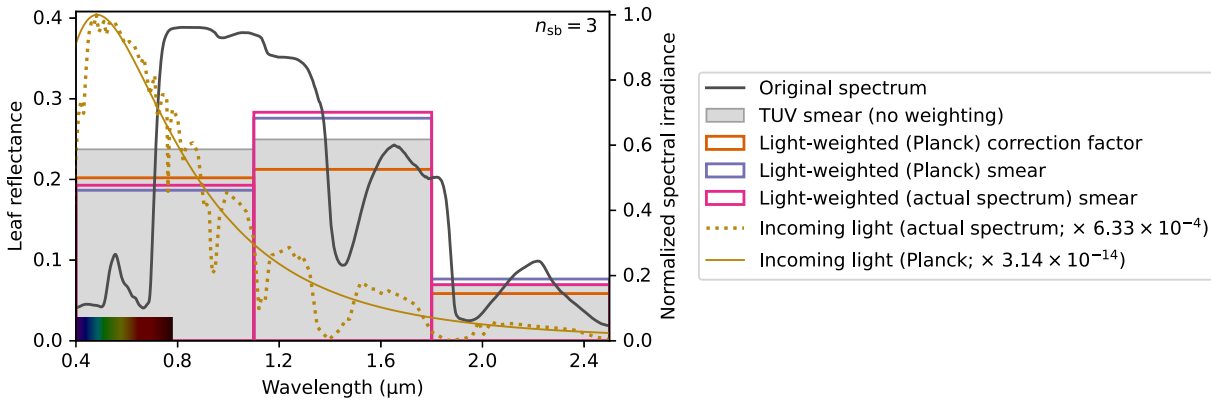

Figure 2. Different methods of binning a leaf optical property (reflectance) spectrum to three equal-width bins over the 0.4–2.5 μm range. The original spectrum is a sample from PROSPECT-5 (the same settings as in PROSPECT-5 online, https://web.archive.org/web/20210618080236/http://opticleaf.ipgp.fr/index.php?page=prospect, but with $c_b = 0$). The units of the light spectra are W m^{-2} μm^{-1}; they have been scaled to the 0–1 range in order to easily compare their shapes. The n_{sb} denotes number of sub-bands of sunlight wavelengths.

where $L(z)$ is the cumulative LAI profile, N the number of interface levels, and subscript m denotes mass or midpoint levels. The heights (z_m) can then be determined by inverting the $L(z)$ function (if using an analytical profile) or by interpolation (if using LAI data for a real canopy).

The layerwise absorbed irradiance is computed by adding up the inputs and subtracting the outputs. Using the symbols of Section 2.1, we have

$$a_m(i) = I_b^{\downarrow}(i+1) - I_b^{\downarrow}(i) + I^{\downarrow}(i+1) - I^{\downarrow}(i) + I^{\uparrow}(i) - I^{\uparrow}(i+1) \tag{12}$$

Note that a_m is defined relative to ground area; to move to leaf-area-relative units, we can divide by the differential leaf area profile ($\delta L(i) = L(i+1) - L(i)$). We can distinguish between sunlit and shaded leaf absorption using the sunlit (f_{sl}) and shaded (f_{sh}) leaf fractions (J. Fuentes et al., 1996):

$$f_{sl} = e^{-K_b L_m}; f_{sh} = 1 - f_{sl} \tag{13}$$

Note that Equation 13 neglects foliage clumping. To consider influences of foliage clumping, it is necessary to use the clumping index whose value can be unity when the spatial foliage distribution is random, <1 when leaves are clumped (typical), or >1 for a regular distribution (Béland & Baldocchi, 2020; Chen et al., 1997; He et al., 2012; Nilson, 1971). We can also distinguish between absorbed direct beam radiation ($a_{m,b}$) and absorbed diffuse ($a_{m,df}$):

$$a_{m,b}(i) = I_b^{\downarrow}(i+1)\left[1 - e^{-K_b dL(i)}\right]\alpha_\ell\,;\; a_{m,df} = a_m - a_{m,b} \tag{14}$$

where $\alpha_\ell = \rho_\ell + \tau_\ell$. The bracketed term is $1 - \tau_b$ and represents the fraction that is not transmitted through a hypothetical black leaf layer.

2.6. Spectral Resolution

As shown in Figure 1c, leaf optical properties are crucially important to reliably estimate the spectral irradiance in plant canopies. The resolution of irradiance waveband to include in the RT methods must be properly represented to capture the variability in the foliage optical properties as a function of sunlight wavelength. Thus, it is necessary to determine the extent of the irradiance waveband to compare results obtained using different spectral resolutions. This requires binning the leaf optical properties, which is a nontrivial problem (Section 2.4). Figure 2 demonstrates four methods (Section 2.4) of binning leaf reflectance from the original spectrum to three equal-width, broad, sub-bands ($n_{sb} = 3$). In the left (0.4–1.1 μm) band, not accounting for the light spectrum shape (optical properties binning method 1; see numbered methods in Section 2.4) leads to an overestimation of the reflectance of about 25%. This overestimation results because the solar spectrum peaks in the visible region as

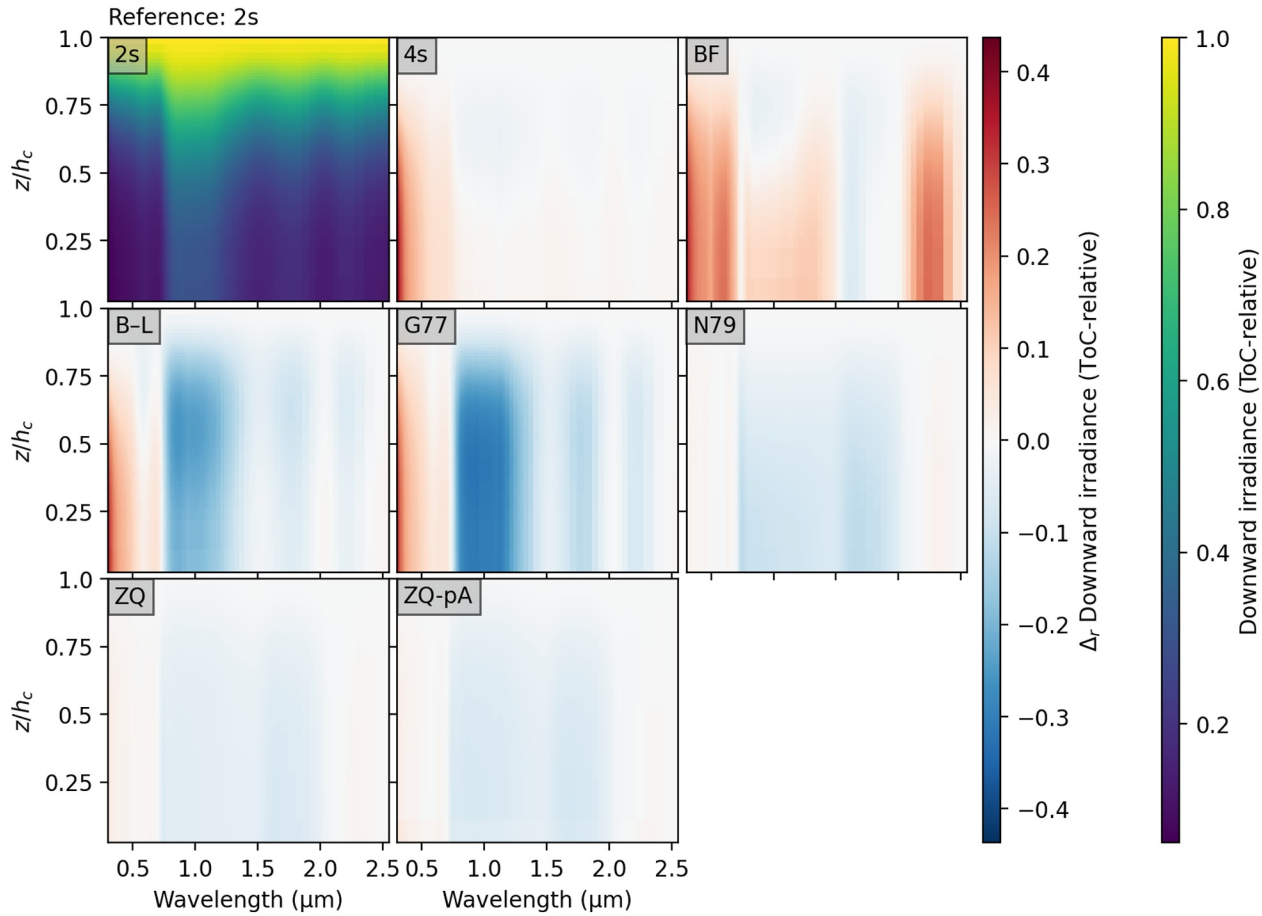

Figure 3. Normalized downward spectral irradiance (unitless), relative to the irradiance at the top of the canopy (ToC). The results for the two-stream model are plotted normally, and those for the other radiative transfer models are plotted as relative difference (Δ_r) with respect to the two-stream approach, where Δ_r implies $\frac{x-x_{\text{Reference}}}{|x_{\text{Reference}}|}$. Figure S1 in Supporting Information S1 provides a larger view of the irradiance profiles computed with the two-stream model.

does light absorption by the leaf. Method 1 weights the reflectance too much toward the high reflectance values in the 0.7–1.1 μm spectral region. Notably, the optical properties binning method 2 produces a value close to those of methods 3 and 4 in this region. In the center (1.1–1.8 μm) band, the leaf reflectance is underestimated by method 1, because here reflectance is greater where solar irradiance is greater. In this band and the right band, the light-weighted correction factor (optical properties binning method 2) makes the reflectance worse. However, the improvement in the left band, which has most of the solar energy, more than compensates for this deficiency. For these broad bands, there is little difference between the light-weighted smearing methods (methods 3 and 4). This suggests that, at least for broad bands, the more computationally efficient and accurate method 3 is comparable to the most-theoretically-sound method 4. This is because variation in the solar spectrum with respect to the Planck curve is mostly smoothed over at this resolution. Thus, we recommend using optical properties binning method 3 unless hyperspectral observations of the incoming light spectra are available. These results (Figure 2) apply to a SZA of 20°, typical for mid-latitude summer conditions around midday.

3. Results

The radiative transfer simulations demonstrate that wavelengths of the light spectrum are not uniformly modified with canopy depth. For example, for the default case (Section 2.2), changes in the light spectrum occur as canopy depth increases (i.e., from $z/h_c = 1$ at the top of the canopy to the ground level at $z/h_c = 0$, Figure 3). Results for the 2s model show (Figure 3) that the light (relative to that at the top of the canopy) is attenuated in all spectral regions, but notably less so in the proximity of the near-IR (0.8–1.2 μm), which is consistent with previous findings (Moon et al., 2020). This result is related to the relatively low leaf absorbance in this spectral region

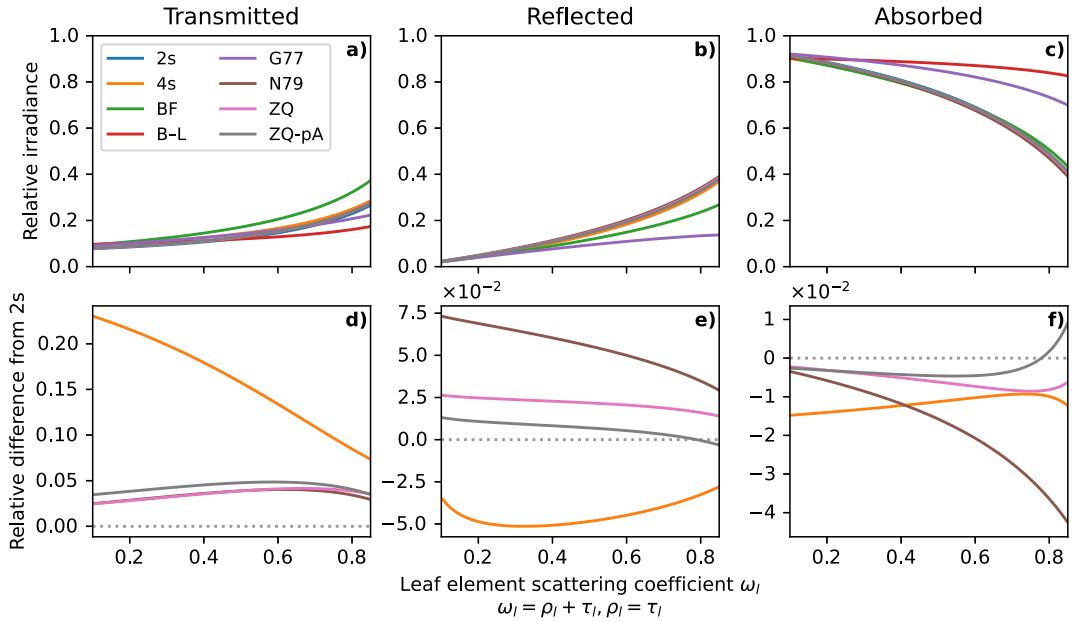

Figure 4. For all canopy radiative transfer models (Table 1), dependence of canopy transmittance, reflectance, and absorption of total solar irradiance on the leaf element scattering coefficient ω_l is shown (a–c). The soil absorption is not included in (c). Leaf reflectance ρ_l and transmittance τ_l were both set to $\omega_l/2$ and the incoming diffuse fraction was 0.5. In the bottom row (d–f), the results for some models are compared to 2s as a relative change $\left(\frac{x-x_{\text{Reference}}}{|x_{\text{Reference}}|}\right)$.

(Figure 1). For the other RT models, the in-canopy light spectrum changes in different ways. Figure 3 illustrates this result by plotting the outputs of the other models as relative differences, with 2s model as the reference. For example, for B–L, G77, N79, ZQ, and ZQ-pA models, the 0.8–1.2 μm region is attenuated more than it is for the 2s method and vice versa for the visible region of the light spectrum. For the B–L model, this result is qualitatively consistent with Y. P. Wang (2003), who found the B–L model to compute less absorption of visible light and more absorption of near-IR than the 2s model for the LAI considered in this study. The extent of the differences is quite RT method-dependent. Differences for N79, ZQ, and ZQ-pA models are ≤5%, whereas for BF, B–L, and G77 methods they can be as high as 30! to 45%. Results for the 4s method are the most similar to the 2s model, except in the smallest wavelengths where the differences approach 25%.

Figure 4 demonstrates, in a simplified setting, why the different RT methods lead to different changes in the light spectrum shape within the canopy. The top row shows how canopy-relative irradiances depend on the leaf optical properties. Relative (to top-of-canopy) transmitted and reflected light both increase with ω_l, the leaf element scattering coefficient, while absorbed light decreases, consistent with theory. The less complex RT models (B–L, BF, G77) stand out as being significantly different from the more complex ones and so are not shown in the second row, which compares the others to 2s using a relative difference metric. For example, the B–L and G77 models both absorb too much light for most of the ω_l range compared to the complex model consensus. Figure 4e explains the differences estimated for the visible region of Figure 3: for small values of leaf reflectance, upward-going light is underpredicted for 2s relative to N79, ZQ, and ZQ-pA models. For high values of leaf reflectance (e.g., 0.8–1.2 μm), the ZQ methods absorb more in the canopy than 2s, whereas N79 and 4s absorb less. For real green leaves, ω_l values are typically within 0.1–0.2 for the visible band and 0.6–0.85 for the near-IR (Asner et al., 1998; Lawrence et al., 2019). For solar irradiance, the average ω_l value is typically between 0.25 and 0.6 (Ross, 1981).

While Figure 4 shows how each RT method's results depend on leaf optical properties, Figure 5 compares the dependence of PAR canopy-level results on SZA. Figure 5a confirms the well-established notion that canopy transmission decreases with SZA, primarily due to the increase in path length through the canopy for the direct solar beam (Moon et al., 2020). At high SZA, differences with respect to the 2s model are greatest, ranging from 5% for the N79 model to 90% for the 4s model calculated transmission. The consensus in sign indicates that the 2s model is underpredicting light transmission for high SZA values. Consistent with radiative transfer theory,

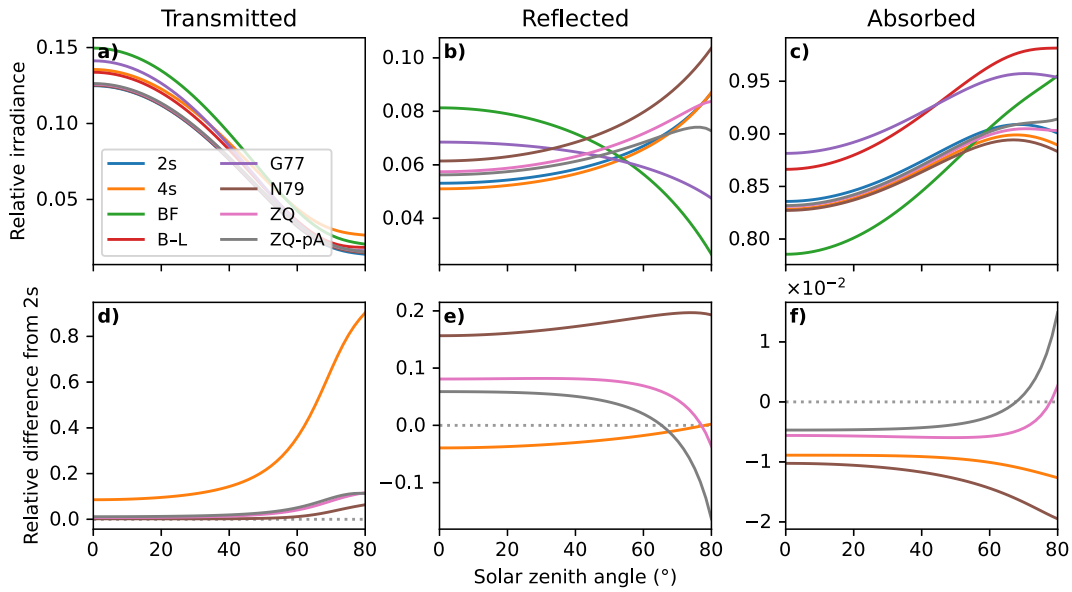

Figure 5. For all canopy RT models (Table 1), dependence of canopy transmittance, reflectance, and absorption of PAR irradiance on the solar zenith angle ψ using the default case (Section 2.2) is shown (a–c). The soil absorption is not included in (c). In the bottom row (d–f), the results for some RT methods are compared to 2s as a relative change $\left(\frac{x-x_{\text{Reference}}}{|x_{\text{Reference}}|}\right)$.

relative reflected and absorbed PAR also generally increase with SZA values due to the longer path length for the direct solar beam. Among the four more complex RT models, the absorption dependency on SZA (Figure 5f) is qualitatively similar to Figure 4f: for high scattering (SZA near 90° or scattering coefficient near 1), the ZQ model predicts more light absorption than the 2s model whereas the N79 and 4s methods predict less.

While Figure 2 presents one binning of leaf reflectance, Figure 6 compares the different optical properties binning methods for a range of equal-width sub-band binnings (1–100 n_{sb}). To do so, we compute the average value of the binned leaf reflectance over the whole range (0.4–2.5 μm as in Figure 2). When computing the average value of the binned leaf reflectance, optical properties binning methods 2 and 3 converge to the same result, so Figure 6 only presents three averaging methods. In each panel, one of the averaging methods gives leaf reflectances that do not vary with n_{sb}. This occurs when the technique used for averaging the binned reflectance spectrum was also used in the binning process. For example, when either of the Planck binning methods are used (optical properties binning method 2 or 3), the Planck-weighted integrated average does not change with n_{sb}. At high n_{sb}, computing the average without light-weighting underpredicts the mean leaf reflectance for this region by almost 0.02 or about 10%. At low n_{sb} when optical properties binning method 1 is used, the large overprediction (0.06 or about 30%) in average reflectance highlights this binning method's misrepresentation of the reflectance spectrum. Regardless of the binning method employed, at sufficiently high n_{sb} (here about 30 sub-bands, or 70 nm), a further increase in spectral resolution has a negligible impact on the average for a given averaging method. For $n_{sb} \leq 8$, though, there is considerable variation in the computed average reflectance in all cases. For optical properties binning method 4, this variation extends to larger n_{sb} related to (mis)alignment of the "dips" (local minima) in the solar spectrum (Figure 2) with the bins being used.

Figure 7 presents the dependence on spectral resolution (n_{sb}) for canopy solar irradiance. As in Figure 6, results for the four optical properties binning methods are shown. Notably, for n_{sb} up to 3, the results are quite different for the standard TUV smear with no light weighting (e.g., >25% greater canopy reflected solar irradiance). This discrepancy is due to the overestimation of optical properties in the visible range as highlighted in Figures 2 and 6 and discussed above. Although it depends somewhat on which variable is examined, beyond $n_{sb} = 10$, differences between the results for the four optical properties binning methods are less appreciable. This is because as n_{sb} increases, results converge to the fully spectrally resolved solution. Taking $n_{sb} = 200$ (the rightmost and largest value in Figure 7) to be "truth," it is apparent that with low spectral resolution, canopy reflected solar irradiance is

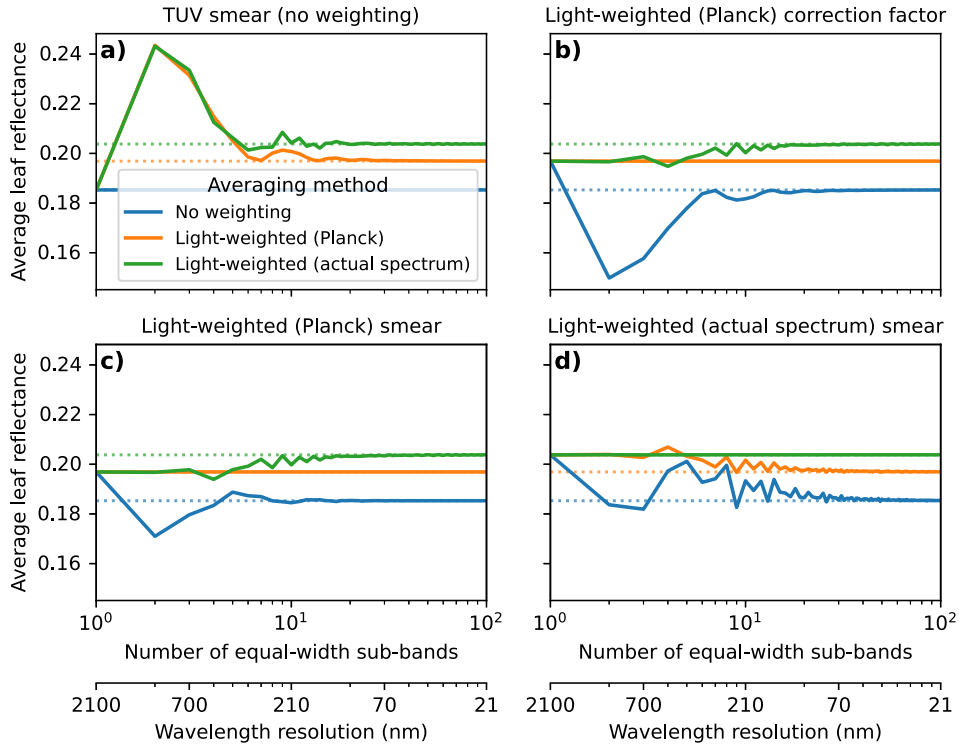

Figure 6. Different methods (each panel) of binning a leaf optical property (reflectance) for different numbers of equal-width sub-bands. Each panel corresponds to a certain optical properties binning method (Section 2.4). In each panel, each line is the average of the binned leaf reflectance over all of the bins (here 0.4–2.5 μm) spectral region computed using a different averaging method (light weighting technique, Section 2.4). The dotted lines are the averages computed using the original spectrum, which has a resolution of 1 nm.

underestimated and canopy absorbed solar irradiance is overestimated (in this example by about 70 W m^{-2} or 38% and 100 W m^{-2} or 16%, respectively).

Much of the dependence on spectral resolution for canopy total solar variables results from the large leaf scattering coefficient values found in certain spectral regions of the near-IR (Figure 6). In the PAR region, light absorption is much more likely. Therefore, improvements in the simulation of light scattering have less of an impact on the results. However, as revealed by results in Figure 8 the canopy reflected PAR is still significantly underestimated when low spectral resolution is used (here by 0.7 W m^{-2} or 5.8%). Canopy absorbed PAR is correspondingly overestimated by about 0.9 W m^{-2}, but this is only 0.3% of the total absorbed PAR.

The remaining panels of Figure 8 examine the impact of spectral resolution on the ratio of photosynthetically active flux density (PPFD) to PAR (irradiance) within the forest canopy. PPFD:PAR depends on the distribution of light intensity within the PAR region. This is an important quantity in plant canopy models because most photosynthesis parameterizations (e.g., Farquhar et al., 1980) use PPFD but most canopy RT schemes output irradiance profiles. Typically, 4.6 PPFD:PAR is used to make the conversion (for PPFD in μmol m^{-2} s^{-1} and PAR in W m^{-2}), corresponding to a median wavelength of 550 nm. However, canopy RT leads to modifications of the median wavelength (Figure S2 in Supporting Information S1). For absorbed direct beam light (Figure 8c), changes in PPFD:PAR with n_{sb} are only minor, though the values are notably all below 4.6. For absorbed diffuse light, however, the PPFD:PAR with high spectral resolution is on average closer to 4.5 than 4.6. Furthermore, there is significant vertical variation of the ratio. In the lowermost canopy region, PPFD:PAR is about 4.71 while near the canopy top it is about 4.46.

Knowledge of the light spectrum is also essential for the computation of photolysis of molecules. Photolysis rate coefficients ("*J*-values"; J_χ, where χ represents the chemical species) express the dependence of these reactions on the light spectrum, specifically the spectral actinic flux. In Figure 9 the impact of spectral resolution on *J*-values for several photolysis reactions is shown. As demonstrated in Moon et al. (2020), photolysis reactions involve

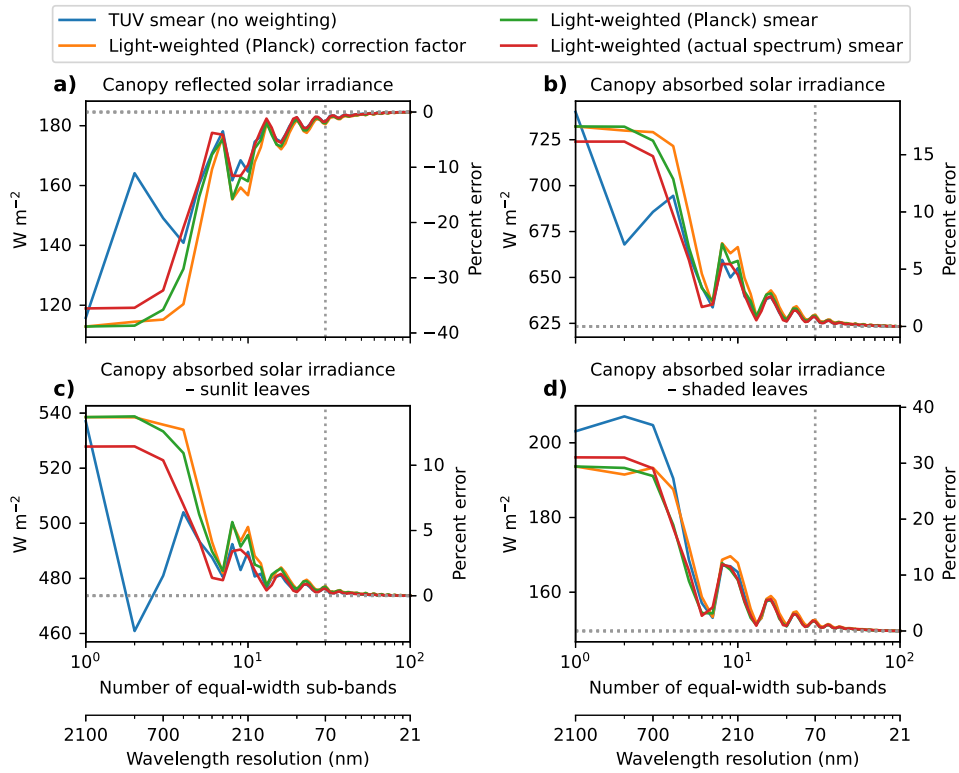

Figure 7. Canopy reflected and absorbed solar irradiance, integrated over the entire 0.4–2.5 μm range (a, b), and canopy absorbed solar irradiance by sunlit and shaded leaves (c, d) for canopy RT using different numbers of equal-width sub-bands. Each color represents one of the four methods (Section 2.4) for binning the leaf and ground surface optical properties.

chemical-species-dependent absorption cross-sections (σ) and reaction-dependent photolysis quantum yields (ϕ), both of which are wavelength-dependent. Absorption cross-sections, in particular, often involve fine-scale features that require high spectral resolution to resolve. For most reactions, the canopy mean relative J-value profile changes only negligibly at a spectral resolution of less than 10 nm (Figure 9). The PAR weighting method,

$$J_\chi(z) = \frac{I_{PAR}(z = h_c)}{I_{PAR}(z)} J_\chi(z = h_c), \tag{15}$$

commonly used in 1-D canopy-chemistry models (e.g., J. D. Fuentes et al., 2007; Moon et al., 2020), introduces positive errors of 20 ! to 25 % for most reactions. This is consistent with the findings of Moon et al. (2020) and results because most photolysis reactions require UV light, and UV actinic light is generally attenuated more readily in the canopy than PAR irradiance (Moon et al., 2020). For photochemical reactions involving ozone, O_3 ($O_3 + h\nu \rightarrow O(^1D)$ or $O_3 + h\nu \rightarrow O$) and nitrate radical, NO_3 ($NO_3 + h\nu \rightarrow NO + O_2$ or $NO_3 + h\nu \rightarrow NO_2 + O$); O is atomic oxygen, $O(^1D)$ is the excited state of atomic oxygen, NO is nitric oxide) that can occur appreciably with visible light, the PAR weighting method slightly underestimates in-canopy photolysis. For these reactions, canopy mean relative J-value increases with n_{sb}, because higher resolution better-resolves the portions of the visible light range of the spectrum where absorption is lower, leading to higher $J(z)/J(h_c)$. For most reactions, however, a weighting method using UV actinic light would be better: the 300–340 nm UV weighting method overestimates the canopy mean relative J-value profile for most reactions by about 2.5%, while the PAR weighting methods overestimate by 26%. These reactions require high-energy UV light, and higher spectral resolution allows the low incoming spectral radiance and high leaf absorption in this spectral region to be resolved better, reducing $J(z)/J(h_c)$. For reactions involving nitrogen dioxide, NO_2 (e.g., $NO_2 + h\nu \rightarrow NO + O$), a spectral resolution of 40 nm is sufficient to obtain errors less than 1%. This result indicates smoother and/or less variable σ and ϕ, such that $\sigma\,\phi$ can be resolved well with fewer wavebands. For other reactions, in particular those that depend mostly on the highest-energy UV light (e.g., $O_3 + h\nu \rightarrow O(^1D)$), a higher waveband resolution is required.

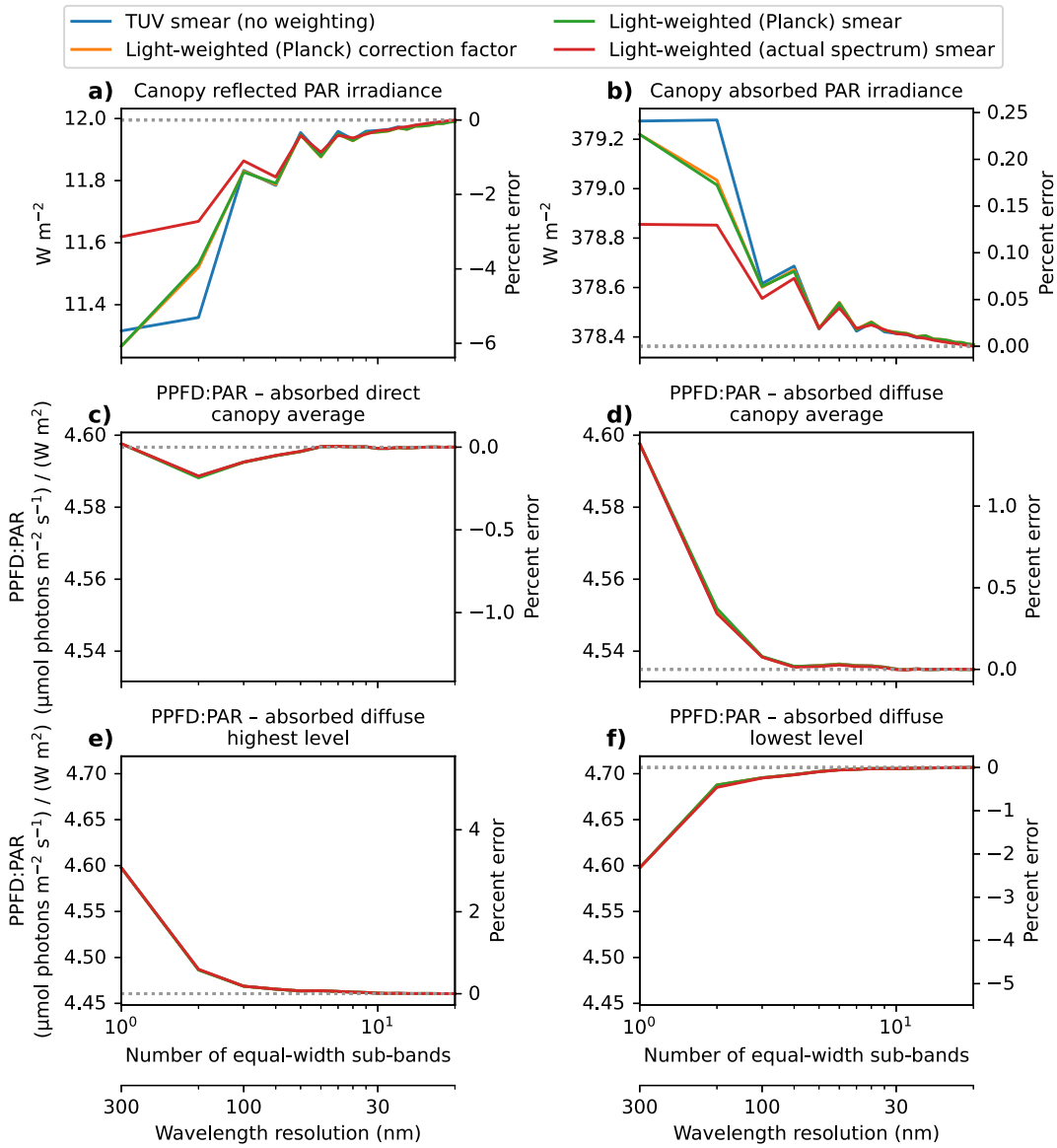

Figure 8. Dependence of PAR (0.4–0.7 μm) quantities on spectral resolution. PPFD: photosynthetically active photon flux density. These include canopy reflected and absorbed PAR irradiance (a, b) and PPFD:PAR for direct and diffuse light averaged over the canopy (c, d) and at the lowest level (e, f). Each color represents one of the four methods for binning the leaf and ground surface optical properties.

The $J(z)/J(h_c)$ values for nitrous acid (HONO) exhibit similar patterns as a function of wavelength compared to those for NO_2 (HONO + hν → NO + OH), OH is the hydroxyl radical). Similarly, the $J(z)/J(h_c)$ values for formaldehyde (HCHO) display comparable patterns to those for O_3 (HCHO + hν → H + HCO), H is the hydrogen atom, HCO is the formyl radical). In summary, a spectral resolution of 10 nm, highlighted in Figure 9, is sufficient to give errors in the photolysis reaction calculations of less than 0.5 % for all reactions shown.

Figure 9 also presents (dotted lines), for selected reactions, the results that occur when σ and ϕ are interpolated (Equation 7) separately and then multiplied before integrating over wavelength limits. The issue with this approach is that $\int \sigma\ \phi\ d\omega$ is not generally equal to $\int \sigma\ d\omega \int \phi\ d\omega$. Numerical models that compute J-values explicitly often use this method (Madronich & Flocke, 1997; Wolfe et al., 2016). However, these models use or expect a high spectral resolution by default (typically <10 nm), so the approach employed in the current study introduces negligible errors (Figure 9). With low spectral resolution, the impact is noticeable for reactions such as O_3 + hν → O + O_2 in particular. For this reaction, σ increases sharply (multiple orders of magnitude) with

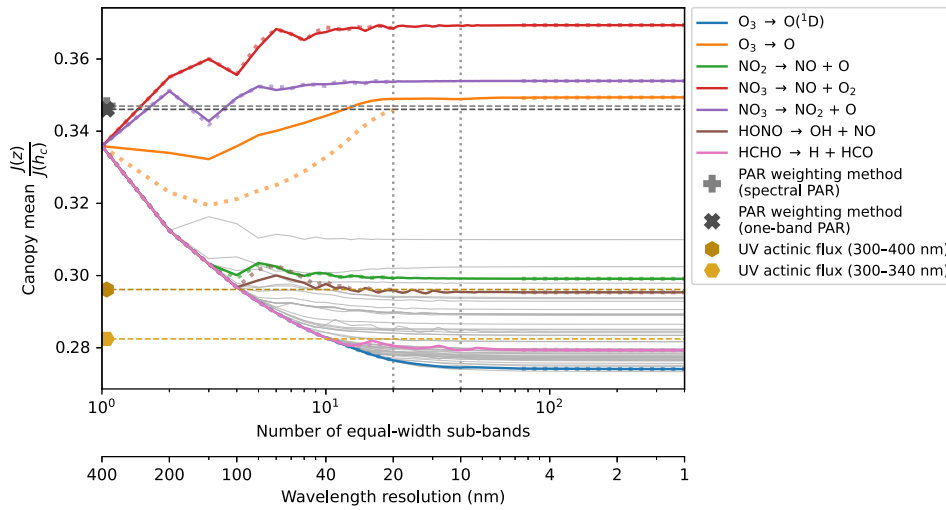

Figure 9. Dependence on spectral resolution for photolysis rate coefficients computed over the 300–700 nm region. Results using OP binning method 2 are shown. $J(z)/J(h_c)$ indicates a relative J-value profile (=1 at $z = h_c$). The thin gray lines are the canopy mean of $J(z)/J(h_c)$ values for individual photolysis reactions. Certain reactions are identified with colored lines. The dotted colored lines indicate results if photolysis quantum yield and absorption cross-section are interpolated (binned) separately before the integration over wavelength to compute the J values. See corresponding plots for different solar zenith angles in Figure S3 in Supporting Information S1.

decreasing wavelength around 380 nm to about 250 nm, while quantum yield of oxygen atoms decreases (Moon et al., 2020). Therefore, interpolating first and multiplying after causes the relative J profile to be underestimated due to over-weighting the UV light by as much as 5% for the case of O_3 photolysis (i.e., $O_3 + h\nu \rightarrow O + O_2$).

4. Discussion

Overall, the comparison to the two-stream approach results indicates a consensus among the more complex group of canopy RT models that explicitly consider the upward radiation stream and include light scattering (i.e., 4s, N79, ZQ, ZQ-pA methods). In particular, the evaluated models are able to better simulate the radiative transfer in the spectrum region of 0.8–1.2 μm where scattering predominates over light absorbance. The differing dependencies on the leaf optical properties among the RT models lead to the differences in in-canopy light spectrum changes as revealed in the results presented in Figure 3. At low solar elevation angles, the RT models (except the 4s method) exhibit deficiencies in properly simulating the in-canopy radiative transfer. This result in part provides the rationale for including more radiation streams (Tian et al., 2007). However, because the incoming solar irradiance is much reduced at this time of the day, the larger relative differences are generally less physically meaningful.

The reliable simulation of spectral irradiance transfer in plant canopies hinges on robust methods to bin the optical properties of foliage. Just like when binning optical properties, computing the average of the binned leaf reflectance over a certain spectral region must incorporate the physical shape of the illuminating light spectrum in some way (Section 2.4). As results indicate (Figure 7), the four binning methods developed in this study provide realistic representation of the light spectra for the chosen subregions of solar irradiance.

The minimum resolution of the waveband to include in RT models is crucially important and depends on the type of processes being investigated. For example, for the estimation of the surface energy balance, based on the results for typical mid-latitude summer noontime conditions, the spectral resolution of about 70 nm is the minimum required to estimate reliable shortwave radiative transfer in plant canopies. For the estimation of photolysis of molecules, the minimum waveband resolution is 10 nm to estimate the necessary spectral actinic resolution involved in the cleavage of molecules. The key results derived from this study is that higher waveband resolution can yield more accurate RT results. However, the computational times to execute the RT models appreciably increase with the number of wavebands.

Although the spectral resolution appears to have a negligible impact on canopy absorbed PAR, improved PPFD:PAR associated with better spectral resolution ratios may impact canopy photosynthesis calculations and consequently gain improved understanding of ecosystem thermodynamics (Lin et al., 2009). Results generated in the current study imply that with a single PAR band, as is commonly done in land models, absorbed diffuse light is likely overestimated by 2! to 5%. This finding is of great importance in the area of carbon assimilation by forested ecosystems as previous studies have posited that having a larger fraction of diffuse light enhances photosynthesis (e.g., Gu et al., 1999; Gu et al., 2002), underscoring the importance of accurately simulating absorbed diffuse PPFD.

5. Conclusions

This study evaluated eight radiative transfer approaches to determine spectral radiative transfer in plant canopies. Model comparisons revealed that the RT approaches that explicitly simulate two streams (upward and downward hemispheres) produced similar results for canopy absorbed (within ±2%) and reflected (within ±5%) sunlight, except for extremely low or high values of leaf element scattering coefficients. Based on the estimated canopy reflected irradiance, the two-stream RT method should be preferred in most cases but especially for high (>80°) zenith solar angles or high leaf scattering coefficients. Radiative transfer methods that do not explicitly treat at least two streams of irradiance should be avoided except for low (<0.2) leaf scattering coefficient conditions.

The current study also provides a new set of strategies for working with light spectra, including special functions for binning irradiance and foliage optical property spectra in order to test the sensitivity of RT model results to spectral resolution. An accurate binning method for foliage optical properties must account for the shape of the impinging sunlight spectrum; we found this to be important for total solar irradiance quantities up to a spectral resolution of about 200 nm. For solar irradiance, a spectral resolution of less than equal to 70 nm is sufficient for computation of reflected and absorbed light. This resolution reduced errors in canopy reflected irradiance from as much as -70 W m^{-2} (-38%) to ~ -1 W m^{-2}. We also found spectral resolution to be important for the PPFD:PAR ratio, which impacts canopy carbon cycle computations and reflected PAR. Despite high absorption by leaves in the visible region of the sunlight spectrum, three or four sub-bands are needed to accurately obtain PPFD:PAR, especially for diffuse light and if the foliage in the plant canopy is vertically resolved. With one PAR band, PPFD:PAR is overestimated for diffuse light, from 2! to 5%, leading to positive errors in PPFD absorption and photosynthetic activity in biophysical models. For in-canopy photolysis rate coefficients (J-values), a waveband resolution of less than equal to 10 nm is sufficient to obtain accurate profiles for all studied photochemical reactions. Compared to the PAR weighting method, positive reaction-dependent errors in canopy-mean relative J-values as high as 30% are reduced to near 0% with the 10 nm resolution.

This study evaluated canopy RT schemes in an idealized shortwave-RT-only framework, with clear skies assumed and only one forest canopy type. Our references to a change in accuracy with spectral resolution are within this framework, with high spectral resolution as the source of truth. How this propagates to model outputs (e.g., from a full canopy model) depends on many factors. In certain contexts or for certain applications, a broadband approach may be sufficient. Nonetheless, the results from this study imply the following recommendations for spectral resolution: ≤70 nm for reliable surface energy balance applications and ≤10 nm for the calculations of photolysis of molecules. It is necessary to have observed canopy profiles of spectral irradiance (which currently do not exist in sufficient quantities) to determine the final test of accuracy of the results presented in the current study.

Data Availability Statement

The CRT1D code is open-source and hosted on GitHub: https://github.com/zmoon/crt1d. The version of the CRT1D codebase applicable to this work was tagged and archived (Moon, 2024). The Application Programming Interface (API) documentation, solver references, input/output variable descriptions, and examples are available

at https://crt1d.readthedocs.io/en/latest/. Each RT method can be executed by following the examples included in the software package. CRT1D is MIT Licensed.

Acknowledgments
Z. Moon and J.D. Fuentes acknowledge support from the NCAS-M (NOAA (National Oceanic and Atmospheric Administration) Center for Atmospheric Sciences and Meteorology), Educational Partnership Program, U.S. Department of Commerce, under Agreement No. NA16SEC4810006-NCAS-M. J.D. Fuentes also acknowledges support from the National Science Foundation (Award 2000403). Gordon Bonan provided many useful Matlab programs with G. Bonan (2019, https://github.com/gbonan/bonanmodeling). Programs and their outputs are available at https://zmoon.github.io/bonanmodeling/. The implementation of Norman (1979) in CRT1D is based on (and tested against) the one included there. The CRT1D also includes the implementation of Zhao and Qualls (2005) from pyAPES (Launiainen et al., 2015, https://github.com/LukeEcomod/pyAPES_skeleton), for comparison against our own implementation. We thank Samuli Launiainen for making this code open-source. We thank two journal reviewers and the Associate Editor who provided outstanding comments to improve the final draft of the manuscript.

References

Ashworth, K., Chung, S. H., Griffin, R. J., Chen, J., Forkel, R., Bryan, A. M., & Steiner, A. L. (2015). FORest Canopy Atmosphere Transfer (FORCAsT) 1.0: A 1-D model of biosphere–atmosphere chemical exchange. *Geoscientific Model Development*, *8*(11), 3765–3784. https://doi.org/10.5194/gmd-8-3765-2015

Asner, G. P., Wessman, C. A., Schimel, D. S., & Archer, S. (1998). Variability in leaf and litter optical properties: Implications for BRDF Model inversions using AVHRR, MODIS, and MISR. *Remote Sensing of Environment*, *63*(3), 243–257. https://doi.org/10.1016/S0034-4257(97)00138-7

Baldocchi, D. D., Matt, D. R., Hutchison, B. A., & McMillen, R. T. (1984). Solar radiation within an oak—Hickory forest: An evaluation of the extinction coefficients for several radiation components during fully-leafed and leafless periods. *Agricultural and Forest Meteorology*, *32*(3), 307–322. https://doi.org/10.1016/0168-1923(84)90056-X

Béland, M., & Baldocchi, D. (2020). Is foliage clumping an outcome of resource limitations within forests? *Agricultural and Forest Meteorology*, *295*, 108185. https://doi.org/10.1016/j.agrformet.2020.108185

Bird, R. E., & Riordan, C. (1986). Simple solar spectral model for direct and diffuse irradiance on horizontal and tilted planes at the Earth's surface for cloudless atmospheres. *Journal of Climate and Applied Meteorology*, *25*(1), 87–97. https://doi.org/10.1175/1520-0450(1986)025⟨0087:SSSMFD⟩2.0.CO;2

Bodin, P., & Franklin, O. (2012). Efficient modeling of sun/shade canopy radiation dynamics explicitly accounting for scattering. *Geoscientific Model Development*, *5*(2), 535–541. https://doi.org/10.5194/gmd-5-535-2012

Bonan, G. (2019). *Climate change and terrestrial ecosystem modeling*. Cambridge University Press. https://doi.org/10.1017/9781107339217

Bonan, G. B., Patton, E. G., Harman, I. N., Oleson, K. W., Finnigan, J. J., Lu, Y., & Burakowski, E. A. (2018). Modeling canopy-induced turbulence in the Earth system: A unified parameterization of turbulent exchange within plant canopies and the roughness sublayer (CLM-ml v0). *Geoscientific Model Development*, *11*(4), 1467–1496. https://doi.org/10.5194/gmd-11-1467-2018

Braghiere, R., Wang, Y., Gagné-Landmann, A., Brodrick, P., Bloom, A., Norton, A., et al. (2023). The importance of hyperspectral soil albedo information for improving earth system model projections. *AGU Advances*, *4*(4), e2023AV000910. https://doi.org/10.1029/2023av000910

Braghiere, R. K., Wang, Y., Doughty, R., Sousa, D., Magney, T., Widlowski, J.-L., et al. (2021). Accounting for canopy structure improves hyperspectral radiative transfer and sun-induced chlorophyll fluorescence representations in a new generation Earth System model. *Remote Sensing of Environment*, *261*, 112497. https://doi.org/10.1016/j.rse.2021.112497

Campbell, G. S., & Norman, J. M. (2012). *An introduction to environmental biophysics* (2nd ed.). Springer Science & Business Media.

Chen, J. M. (1996). Canopy architecture and remote sensing of the fraction of photosynthetically active radiation absorbed by boreal conifer forests. *IEEE Transactions on Geoscience and Remote Sensing*, *34*(6), 1353–1368. https://doi.org/10.1109/36.544559

Chen, J. M., Rich, P. M., Gower, S. T., Norman, J. M., & Plummer, S. (1997). Leaf area index of boreal forests: Theory, techniques, and measurements. *Journal of Geophysical Research*, *102*(D24), 29429–29443. https://doi.org/10.1029/97JD01107

Dickinson, R. E. (1983). Land surface processes and climate—Surface albedos and energy balance. *Advances in Geophysics*, *25*, 305–353. https://doi.org/10.1016/S0065-2687(08)60176-4

Farquhar, G. D., von Caemmerer, S., & Berry, J. A. (1980). A biochemical model of photosynthetic CO_2 assimilation in leaves of C_3 species. *Planta*, *149*(1), 78–90. https://doi.org/10.1007/BF00386231

Feret, J.-B., François, C., Asner, G. P., Gitelson, A. A., Martin, R. E., Bidel, L. P. R., et al. (2008). PROSPECT-4 and 5: Advances in the leaf optical properties model separating photosynthetic pigments. *Remote Sensing of Environment*, *112*(6), 3030–3043. https://doi.org/10.1016/j.rse.2008.02.012

Forkel, R., Klemm, O., Graus, M., Rappenglück, B., Stockwell, W. R., Grabmer, W., et al. (2006). Trace gas exchange and gas phase chemistry in a Norway spruce forest: A study with a coupled 1-dimensional canopy atmospheric chemistry emission model. *Atmospheric Environment*, *40*(1), 28–42. https://doi.org/10.1016/j.atmosenv.2005.11.070

Fuentes, J., Wang, D., Neumann, H., Gillespie, T., Den Hartog, G., & Dann, T. (1996). Ambient biogenic hydrocarbons and isoprene emissions from a mixed deciduous forest. *Journal of Atmospheric Chemistry*, *25*(1), 67–95. https://doi.org/10.1007/bf00053286

Fuentes, J. D., Gerken, T., Chamecki, M., Stoy, P., Freire, L., & Ruiz-Plancarte, J. (2022). Turbulent transport and reactions of plant-emitted hydrocarbons in an Amazonian rain forest. *Atmospheric Environment*, *279*, 119094. https://doi.org/10.1016/j.atmosenv.2022.119094

Fuentes, J. D., Wang, D., Bowling, D. R., Potosnak, M., Monson, R. K., Goliff, W. S., & Stockwell, W. R. (2007). Biogenic hydrocarbon chemistry within and above a mixed deciduous forest. *Journal of Atmospheric Chemistry*, *56*(2), 165–185. https://doi.org/10.1007/s10874-006-9048-4

Gao, W., Wesely, M. L., & Doskey, P. V. (1993). Numerical modeling of the turbulent diffusion and chemistry of NO_x, O_3, isoprene, and other reactive trace gases in and above a forest canopy. *Journal of Geophysical Research*, *98*(D10), 18339–18353. https://doi.org/10.1029/93JD01862

Goudriaan, J. (1977). *Crop micrometeorology: A simulation study (unpublished doctoral dissertation)*. Pudoc.

Govaerts, Y., & Verstraete, M. (1998). Raytran: A Monte Carlo ray-tracing model to compute light scattering in three-dimensional heterogeneous media. *IEEE Transactions on Geoscience and Remote Sensing*, *36*(2), 493–505. https://doi.org/10.1109/36.662732

Gu, L., Baldocchi, D., Verma, S. B., Black, T. A., Vesala, T., Falge, E. M., & Dowty, P. R. (2002). Advantages of diffuse radiation for terrestrial ecosystem productivity. *Journal of Geophysical Research*, *107*(D6), ACL2-1–ACL2-23. https://doi.org/10.1029/2001JD001242

Gu, L., Fuentes, J. D., Shugart, H. H., Staebler, R. M., & Black, T. A. (1999). Responses of net ecosystem exchanges of carbon dioxide to changes in cloudiness: Results from two North American deciduous forests. *Journal of Geophysical Research*, *104*(D24), 31421–31434. https://doi.org/10.1029/1999JD901068

Gu, L., Han, J., Wood, J. D., Chang, C. Y.-Y., & Sun, Y. (2019). Sun-induced Chl fluorescence and its importance for biophysical modeling of photosynthesis based on light reactions. *New Phytologist*, *223*(3), 1179–1191. https://doi.org/10.1111/nph.15796

He, L., Chen, J. M., Pisek, J., Schaaf, C. B., & Strahler, A. H. (2012). Global clumping index map derived from the MODIS BRDF product. *Remote Sensing of Environment*, *119*, 118–130. https://doi.org/10.1016/j.rse.2011.12.008

Hogan, R. J., Quaife, T., & Braghiere, R. (2018). Fast matrix treatment of 3-D radiative transfer in vegetation canopies: Spartacus-vegetation 1.1. *Geoscientific Model Development*, *11*(1), 339–350. https://doi.org/10.5194/gmd-11-339-2018

Hu, X.-M., Fuentes, J. D., Toohey, D., & Wang, D. (2015). Chemical processing within and above a loblolly pine forest in North Carolina, USA. *Journal of Atmospheric Chemistry*, *72*(3–4), 235–259. https://doi.org/10.1007/s10874-013-9276-3

Iacono, M. J., Delamere, J. S., Mlawer, E. J., Shephard, M. W., Clough, S. A., & Collins, W. D. (2008). Radiative forcing by long-lived greenhouse gases: Calculations with the AER radiative transfer models. *Journal of Geophysical Research*, *113*(D13), D13103. https://doi.org/10.1029/2008JD009944

Irmak, S., & Mutiibwa, D. (2008). Dynamics of photosynthetic photon flux density and light extinction coefficient to assess radiant eEnergy interactions for maize canopy. *Transactions of the ASABE*, *51*(5), 1663–1673. https://doi.org/10.13031/2013.25323

Jacquemoud, S., & Baret, F. (1990). PROSPECT: A model of leaf optical properties spectra. *Remote Sensing of Environment*, *34*(2), 75–91. https://doi.org/10.1016/0034-4257(90)90100-Z

Jacquemoud, S., Verhoef, W., Baret, F., Bacour, C., Zarco-Tejada, P. J., Asner, G. P., et al. (2009). PROSPECT+SAIL models: A review of use for vegetation characterization. *Remote Sensing of Environment*, *113*(1), S56–S66. https://doi.org/10.1016/j.rse.2008.01.026

Kivalov, S. N., & Fitzjarrald, D. R. (2018). Quantifying and modelling the effect of cloud shadows on the surface irradiance at tropical and midlatitude forests. *Boundary-Layer Meteorology*, *166*(2), 165–198. https://doi.org/10.1007/s10546-017-0301-y

Kivalov, S. N., & Fitzjarrald, D. R. (2019). Observing the whole-canopy short-term dynamic response to natural step changes in incident light: Characteristics of tropical and temperate forests. *Boundary-Layer Meteorology*, *173*, 1–52. https://doi.org/10.1007/s10546-019-00460-5

Launiainen, S., Katul, G. G., Lauren, A., & Kolari, P. (2015). Coupling boreal forest CO_2, H_2O and energy flows by a vertically structured forest canopy – Soil model with separate bryophyte layer. *Ecological Modelling*, *312*, 385–405. https://doi.org/10.1016/j.ecolmodel.2015.06.007

Lawrence, D. M., Fisher, R. A., Koven, C. D., Oleson, K. W., Swenson, S. C., Bonan, G., et al. (2019). The Community Land Model Version 5: Description of new features, benchmarking, and impact of forcing uncertainty. *Journal of Advances in Modeling Earth Systems*, *11*(12), 4245–4287. https://doi.org/10.1029/2018MS001583

Lin, H., Cao, M., Stoy, P. C., & Zhang, Y. (2009). Assessing self-organization of plant communities—A thermodynamic approach. *Ecological Modelling*, *220*(6), 784–790. https://doi.org/10.1016/j.ecolmodel.2009.01.003

Madronich, S., & Flocke, S. (1997). Theoretical estimation of biologically effective UV Radiation at the Earth's surface. In C. S. Zerefos & A. F. Bais (Eds.), *Solar ultraviolet radiation* (pp. 23–48). Springer Berlin Heidelberg.

Makar, P. A., Fuentes, J. D., Wang, D., Staebler, R. M., & Wiebe, H. A. (1999). Chemical processing of biogenic hydrocarbons within and above a temperate deciduous forest. *Journal of Geophysical Research*, *104*(D3), 3581–3603. https://doi.org/10.1029/1998JD100065

Mohammed, G. H., Colombo, R., Middleton, E. M., Rascher, U., van der Tol, C., Nedbal, L., et al. (2019). Remote sensing of solar-induced chlorophyll fluorescence (SIF) in vegetation: 50 years of progress. *Remote Sensing of Environment*, *231*, 111177. https://doi.org/10.1016/j.rse.2019.04.030

Monteith, J. L., & Unsworth, M. H. (2013). *Principles of environmental physics: Plants, animals, and the atmosphere* (4th ed.). Academic Press.

Moon, Z. (2024). zmoon/crt1d: v0.2 [Software]. *Zenodo*. https://doi.org/10.5281/zenodo.10869933

Moon, Z., Fuentes, J. D., & Staebler, R. M. (2020). Impacts of spectrally resolved irradiance on photolysis frequency calculations within a forest canopy. *Agricultural and Forest Meteorology*, *291*, 108012. https://doi.org/10.1016/j.agrformet.2020.108012

Neumann, H., Den Hartog, G., & Shaw, R. (1989). Leaf area measurements based on hemispheric photographs and leaf-litter collection in a deciduous forest during autumn leaf-fall. *Agricultural and Forest Meteorology*, *45*(3–4), 325–345. https://doi.org/10.1016/0168-1923(89)90052-x

Nilson, T. (1971). A theoretical analysis of the frequency of gaps in plant stands. *Agricultural Meteorology*, *8*, 25–38. https://doi.org/10.1016/0002-1571(71)90092-6

Norman, J. M. (1979). Modeling the complete crop canopy. In *Modification of the aerial environment of crops* (pp. 249–277). American Society of Agricultural Engineers.

Ollinger, S. V., & Smith, M.-L. (2005). Net primary production and canopy nitrogen in a temperate forest landscape: An analysis using imaging spectroscopy, modeling and field data. *Ecosystems*, *8*(7), 760–778. https://doi.org/10.1007/s10021-005-0079-5

Parker, G. G., Fitzjarrald, D. R., & Sampaio, I. C. G. (2019). Consequences of environmental heterogeneity for the photosynthetic light environment of a tropical forest. *Agricultural and Forest Meteorology*, *278*, 107661. https://doi.org/10.1016/j.agrformet.2019.107661

Press, W. H. (2007). *Numerical recipes: The art of scientific computing* (3rd ed.). Cambridge university press.

Ross, J. (1981). *The radiation regime and architecture of plant stands*. Springer.

Saylor, R. D. (2013). The atmospheric chemistry and canopy exchange simulation system (ACCESS): Model description and application to a temperate deciduous forest canopy. *Atmospheric Chemistry and Physics*, *13*(2), 693–715. https://doi.org/10.5194/acp-13-693-2013

Sellers, P. J. (1985). Canopy reflectance, photosynthesis and transpiration. *International Journal of Remote Sensing*, *6*(8), 1335–1372. https://doi.org/10.1080/01431168508948283

Serbin, S. P., & Townsend, P. A. (2020). Scaling functional traits from leaves to canopies. In J. Cavender-Bares, J. A. Gamon, & P. A. Townsend (Eds.), *Remote sensing of plant biodiversity* (pp. 43–82). Springer International Publishing. https://doi.org/10.1007/978-3-030-33157-3_3

Staebler, R., Fuentes, J., Neumann, H., & Chen, J. (1997). Light interception by a temperate deciduous forest. In *Conference on atmospheric radiation* (Vol. 9, pp. 459–461).

Stroud, C., Makar, P., Karl, T., Guenther, A., Geron, C., Turnipseed, A., et al. (2005). Role of canopy-scale photochemistry in modifying biogenic-atmosphere exchange of reactive terpene species: Results from the CELTIC field study. *Journal of Geophysical Research*, *110*(D17), D17303. https://doi.org/10.1029/2005JD005775

Tian, Y., Dickinson, R. E., & Zhou, L. (2007). Four-stream isosector approximation for canopy radiative transfer. *Journal of Geophysical Research*, *112*(D4), D04107. https://doi.org/10.1029/2006JD007545

van der Tol, C., Verhoef, W., Timmermans, J., Verhoef, A., & Su, Z. (2009). An integrated model of soil-canopy spectral radiances, photosynthesis, fluorescence, temperature and energy balance. *Biogeosciences*, *6*(12), 3109–3129. https://doi.org/10.5194/bg-6-3109-2009

Vane, G., & Goetz, A. F. (1988). Terrestrial imaging spectroscopy. *Remote Sensing of Environment*, *24*(1), 1–29. https://doi.org/10.1016/0034-4257(88)90003-X

Verhoef, W. (1984). Light scattering by leaf layers with application to canopy reflectance modeling: The SAIL model. *Remote Sensing of Environment*, *16*(2), 125–141. https://doi.org/10.1016/0034-4257(84)90057-9

Wang, Y., Köhler, P., He, L., Doughty, R., Braghiere, R. K., Wood, J. D., & Frankenberg, C. (2021). Testing stomatal models at the stand level in deciduous angiosperm and evergreen gymnosperm forests using CliMA Land (v0.1). *Geoscientific Model Development*, *14*(11), 6741–6763. https://doi.org/10.5194/gmd-14-6741-2021

Wang, Y. P. (2003). A comparison of three different canopy radiation models commonly used in plant modelling. *Functional Plant Biology*, *30*(2), 143–152. https://doi.org/10.1071/fp02117

Widlowski, J.-L., Mio, C., Disney, M., Adams, J., Andredakis, I., Atzberger, C., et al. (2015). The fourth phase of the radiative transfer model intercomparison (RAMI) exercise: Actual canopy scenarios and conformity testing. *Remote Sensing of Environment*, *169*, 418–437. https://doi.org/10.1016/j.rse.2015.08.016

Widlowski, J.-L., Pinty, B., Clerici, M., Dai, Y., Kauwe, M. D., de Ridder, K., et al. (2011). RAMI4PILPS: An intercomparison of formulations for the partitioning of solar radiation in land surface models. *Journal of Geophysical Research*, *116*(G2), G02019. https://doi.org/10.1029/2010JG001511

Widlowski, J.-L., Taberner, M., Pinty, B., Bruniquel-Pinel, V., Disney, M., Fernandes, R., et al. (2007). Third radiation transfer model intercomparison (RAMI) exercise: Documenting progress in canopy reflectance models. *Journal of Geophysical Research*, *112*(D9), D09111. https://doi.org/10.1029/2006JD007821

Wolfe, G. M., Marvin, M. R., Roberts, S. J., Travis, K. R., & Liao, J. (2016). The framework for 0-D atmospheric modeling (F0AM) v3.1. *Geoscientific Model Development*, *9*(9), 3309–3319. https://doi.org/10.5194/gmd-9-3309-2016

Wolfe, G. M., & Thornton, J. A. (2011). The chemistry of atmosphere-forest exchange (CAFE) model – Part 1: Model description and characterization. *Atmospheric Chemistry and Physics*, *11*(1), 77–101. https://doi.org/10.5194/acp-11-77-2011

Yang, P., Verhoef, W., & van der Tol, C. (2017). The mSCOPE model: A simple adaptation to the SCOPE model to describe reflectance, fluorescence and photosynthesis of vertically heterogeneous canopies. *Remote Sensing of Environment*, *201*, 1–11. https://doi.org/10.1016/j.rse.2017.08.029

Yang, X., Li, R., Jablonski, A., Stovall, A., Kim, J., Yi, K., et al. (2023). Leaf angle as a leaf and canopy trait: Rejuvenating its role in ecology with new technology. *Ecology Letters*, *26*(6), 1005–1020. https://doi.org/10.1111/ele.14215

Zhao, W., & Qualls, R. J. (2005). A multiple-layer canopy scattering model to simulate shortwave radiation distribution within a homogeneous plant canopy. *Water Resources Research*, *41*(8), W08409. https://doi.org/10.1029/2005WR004016